THE JOURNAL OF PHYSICAL CHEMISTRY C

Article

Cite This: J. Phys. Chem. C 2018, 122, 24512−24519

pubs.acs.org/JPCC

Improved H_2 Evolution in Quaternary SCIGS Chalcopyrite Semiconductors

Danrui Ni, Hsin-Ya Kuo, James Eujin Park, Tia S. Lee, Spyder-Rider I. Sloman, Robert J. Cava,* and Andrew B. Bocarsly*

Department of Chemistry, Princeton University, Princeton, New Jersey 08544, United States

Supporting Information

ABSTRACT: In a search for improved photocathode materials for fuel-producing photoelectrochemical cells, quaternary $Ag_xCu_{1-x}Ga_yIn_{1-y}S_2$ ($0 \le x \le 1.0$, $0 \le y \le 1.0$) p-type, chalcopyrite semiconductors (SCIGS) were prepared and tested for photochemical hydrogen evolution. The study reported here is based on the preparation of bulk phases of the quaternary system. In contrast to thin-film studies of this system, this approach enables enhanced control of the materials' chemical, structural, and electronic properties. Compared to ternary CIGS electrode materials, the quaternary SCIGS materials provide improved photoelectrochemical and electrocatalytic properties. The quaternary system allows for adjustment of the band structures and photocatalytic abilities to a finer degree than is possible in the $Ag_xCu_{1-x}GaS_2$ or $Ag_xCu_{1-x}InS_2$ ternaries, and several of the quaternary $Ag_xCu_{1-x}Ga_yIn_{1-y}S_2$ compositions are found to show better water-splitting capability than the ternaries, even when a platinum co-catalyst is present in the ternary systems. Our work on quaternary compounds has led to finding unexpected optoelectric properties in ternary compounds of composition $Ag_xCu_{1-x}GaS_2$. Specifically, a "V-shaped" plot of semiconductor composition versus band gap is observed, which is not easily correlated with the observed variation in semiconductor structure. Even more interesting is the observation that the silver-rich branch of this "V" produces obviously higher H_2 evolution rates than observed with the copper-rich branch.

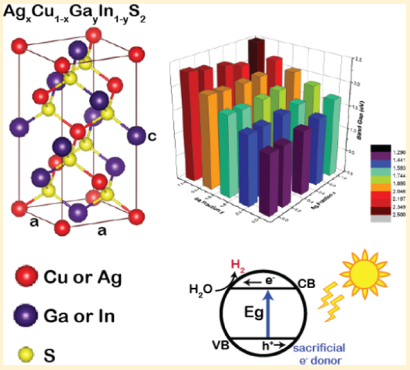

INTRODUCTION

Photochemical and photoelectrochemical water splitting using semiconductor materials has been widely studied since Honda and Fujishima's 1972 report that n-TiO_2 photoanodes were capable of water oxidation.[1] In the intervening time period, various semiconductor materials have been reported as powdered photocatalysts for water splitting under light irradiation including oxides, oxynitrides, chalcogenides, and their solid solutions.[2−6] Visible-light-responsive n-type semiconductor photoanodes have also been prepared to split water.[7−20] Photocathodes based on p-type semiconductors such as $CuRhO_2$ and $AgRhO_2$ have recently been reported;[21,22] however, significantly fewer examples of these materials are known.

Among the candidates for improved water-splitting photocathodes, moderate-band-gap ternary chalcopyrites having a I−III−VI_2 stoichiometry are a promising class of semiconductors for photoelectrochemical water-splitting applications. These materials have been studied primarily in a thin-film format deposited on cathode surfaces.[23] Many I−III−VI_2 materials have light-absorption profiles well-matched to the solar spectrum on the earth, a band gap that straddles the reduction potential of H^+ to H_2 (E^o_R = 0.00 V vs NHE) and the oxidation potential of H_2O to O_2 (E^o_R = 1.23 V vs NHE),[24] and reasonable stability in aqueous electrolytes. Specifically, copper−indium−gallium (CIGS) and silver−indium−gallium (SIGS) chalcogenides are attractive because of their ideal, tunable light-absorption properties and band-edge positions.[25] Several studies have been performed on CIGS- and SIGS-based thin-film electrodes, investigating their activities in photochemical or photoelectrochemical hydrogen evolution,[24,26,27] as well as application in photovoltaic cells.[28−30]

The ternary CIGS and SIGS systems can be considered the end points of a larger family of quaternary materials in which the ratio of the Group IB metal cations (i.e., Cu and Ag) is varied. Recently, several first-principles density functional theory studies showed potential for further optimization of photochemical water splitting by CIGS/SIGS quaternary materials through changing the chemical constituents on both the IB and IIIB metal sites.[31,32] These calculations indicated that the band-gap values and band-edge positions of the CIGS/SIGS quaternaries change when varying the composition of metal sites because of variations in the I−VI and III−VI band interactions, which are primarily responsible for the valence band maximum (VBM) and the conduction band minimum (CBM), respectively. This reveals an approach to shifting both band-edge positions and modifying the band structures by changing both the Ag to Cu ratio and the Ga to

Received: June 5, 2018
Revised: September 25, 2018
Published: September 26, 2018

DOI: 10.1021/acs.jpcc.8b05389
J. Phys. Chem. C 2018, 122, 24512−24519

In ratio, in other words, expanding the currently studied ternary materials to the full family of quaternary "SCIGS" semiconductors. Within this materials' "genome", one can anticipate finding chalcopyrites with suitable band-gap and band-edge positions that straddle the water redox potentials, allowing in principle for efficient photochemical water-splitting chemistry. Recently, $Ag_xCu_{1-x}Ga_{0.25}In_{0.75}S_2$ thin-film electrodes were prepared over a limited compositional range ($0 \le x \le 0.3$),[33] however, leaving substantial need for further exploration. This goal motivates the present study of quaternary $(Ag,Cu)(Ga,In)S_2$ semiconductors having the chalcopyrite crystal structure and a compositional range that bridges the complete stoichiometry of IB and IIIB cation sites.

For the purposes of this initial investigation, materials were synthesized as powders and evaluated for water reduction under purely photochemical (i.e., not photoelectrochemical) conditions. We find this screen as an efficient methodology for vetting a relatively large number of materials rapidly. Also, the screen of the $(Ag,Cu)(Ga,In)S_2$ family revealed that some of the quaternary materials do indeed display photocatalytic properties and stabilities that are superior to the ternaries. The optimal properties are obtained for quaternary compositions near $Ag_{0.75}Cu_{0.25}Ga_{0.25}In_{0.75}S_2$. These materials show photocatalytic hydrogen evolution performance that is comparable to that of ternaries that are noble-metal-loaded.

EXPERIMENTAL METHODS

Preparation of $(Ag,Cu)(Ga,In)S_2$ Semiconductors. Polycrystalline $(Ag,Cu)(Ga,In)S_2$ semiconductors were prepared by the solid-state reaction method. Stoichiometric amounts of Cu (Alfa Aesar, 99.999% pure), Ag (Alfa Aesar, 99.999% pure), Ga_2S_3 (Alfa Aesar, 99.999% pure), and In_2S_3 (Alfa Aesar, 99.999% pure) were mixed with elemental sulfur (Alfa Aesar, 99.98%, 5% excess, dried at 120 °C overnight before use) and sealed in a quartz ampoule after evacuation. The mixture of starting materials was heated at 900−1000 °C for 72 h. At the end of this time period, the furnace was cooled to room temperature at 3 °C per hour. No further treatment of the samples was found necessary.

Characterization. The prepared polycrystalline semiconductor powders were characterized by powder X-ray diffraction (XRD) using a Bruker D8 Discover X-ray diffractometer with Cu Kα radiation (λ = 0.15415 nm). Lattice parameters were determined based on least-squares fits to the powder XRD patterns by using the Topas diffraction suite. Particle morphology was investigated using an FEI XL30 field-emission gun scanning electron microscope (SEM) equipped with an Oxford X-Max 20 energy-dispersive X-ray (EDX) spectroscopy running on INCA software. Diffuse reflectance spectra were collected by a Cary 6000i UV−vis−NIR spectrometer equipped with an integrating sphere and were converted from reflectance to absorbance using the Kubelka−Munk method.[34] The ultraviolet photoelectron spectroscopy (UPS) measurements were performed on a ThermoFisher K-Alpha + X-ray photoelectron spectrometer (XPS/UPS) using the He I (21.2 eV) line.

Photocatalytic Reactions. To achieve high-throughput screening, all photocatalytic reactions were carried out on a homemade light table to ensure concurrent and uniform irradiation. Every photocatalytic hydrogen evolution cell consisted of a 15 mL clear borosilicate glass vial sealed with a polytetrafluoroethylene/silicone septum (Supleco). A weighed amount of photocatalyst powder (ca. 20 mg) was dispersed in 5 mL of aqueous solution containing Na_2S (sodium sulfide nanohydrate, ≥98%, 208043 Sigma-Aldrich) and/or Na_2SO_3 as sacrificial electron donors. The photocatalysts were irradiated with 365 nm light from a 3 W light-emitting diode (LED). The light source intensity and vial-to-light-source distance was held constant for all samples using a machined aluminum fixture based on the Bernhard design.[35] Hydrogen product analysis was carried out by gas chromatography. A gas tight syringe was used to withdraw 50 μL of gas from the vial headspace. Samples were analyzed using an SRI 8610C gas chromatograph with a thermal conductivity detector and a Molsieve column (HAYESEP D) with Ar flow gas.

In some cases, the particles were coated with platinum particles as a co-catalyst. To this end, Pt was photodeposited in situ from an 8 wt % concentration of aqueous H_2PtCl_6.[36,37]

RESULTS AND DISCUSSION

Preparation and Characterization of $Ag_xCu_{1-x}Ga_yIn_{1-y}S_2$ ($0 \le x \le 1.0$, $0 \le y \le 1.0$). Figure 1 shows representative powder XRD patterns for the synthesized $Ag_xCu_{1-x}GaS_2$ (x = 0, 0.2, 0.4, 0.6, 0.8 and 1.0) and $Ag_{0.5}Cu_{0.5}Ga_yIn_{1-y}S_2$ (y = 0, 0.25, 0.5, 0.75 and 1.0) chalcopyrites. A full library of XRD patterns obtained in this work is presented in Figures S1−S5. Compared with the

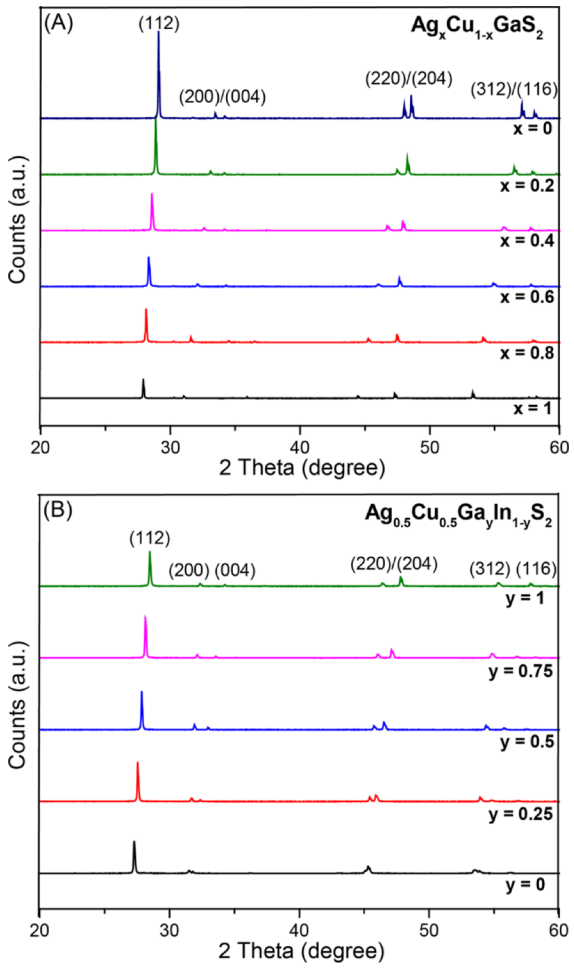

Figure 1. Representative powder XRD patterns of (A) $Ag_xCu_{1-x}GaS_2$ for x = 0, 0.2, 0.4, 0.6, 0.8, and 1 and (B) $Ag_{0.5}Cu_{0.5}Ga_yIn_{1-y}S_2$ for y = 0, 0.25, 0.5, 0.75, and 1.

DOI: 10.1021/acs.jpcc.8b05389
J. Phys. Chem. C 2018, 122, 24512−24519

previous preparation of quaternary semiconductor thin films,[33] the bulk materials presented here dramatically widen the compositional range of the quaternary system, through variation of both x and y stoichiometric parameters. No secondary phases were observed, indicating the successful formation of quaternary $Ag_xCu_{1-x}Ga_yIn_{1-y}S_2$ solid solutions. The diffraction features can be consistently indexed to a tetragonal unit cell as shown in Figure 1, based on the unit cell structure shown in Figure 2. The diffraction peaks shift

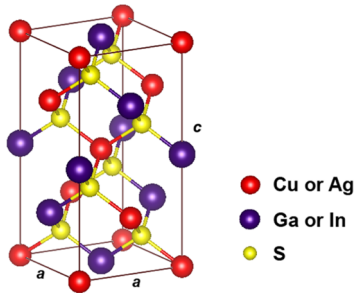

Figure 2. Chalcopyrite unit cell of CIGS/SIGS materials, labeled with lattice parameters a and c. The red spheres represent Ag and Cu, the purple spheres represent Ga and In, and the yellow spheres represent S.

systematically with different Ag to Cu and Ga to In ratios, reflecting the variation of lattice parameters because of the differences in ionic radii between Ag^+ (1.00 Å) and Cu^+ (0.60 Å) or Ga^{3+} (0.47 Å) and In^{3+} (0.62 Å).[27]

Table 1 correlates changes in the observed lattice parameters and measured band gaps with stoichiometry in the quaternary

Table 1. Variation with Composition of the Lattice Parameters a and c for the Tetragonal Unit Cell and the Band Gap E_g for $Ag_xCu_{1-x}Ga_yIn_{1-y}S_2$

x	y	a (Å)[a]	c (Å)[a]	E_g (eV)[b]
0	1	5.360(2)	10.495(7)	2.34
0.2	1	5.414(5)	10.505(7)	2.28
0.5	1	5.531(6)	10.482(3)	2.21
1	1	5.765(5)	10.315(9)	2.50
0	0.5	5.442(6)	10.840(7)	1.74
0.9	0.5	5.776(8)	10.795(7)	1.78
0.2	0.25	5.546(2)	11.041(8)	1.52
0.5	0.25	5.648(5)	11.066(2)	1.56
0.5	0	5.685(5)	11.269(8)	1.37

[a]Lattice parameters were determined based on least-squares fits to the powder XRD patterns by using the Topas diffraction suite. [b]Derived from UV−vis diffuse reflectance spectroscopy by extrapolating the linear part of the $(\alpha h\nu)^2$ vs $h\nu$ based on eq 1 for direct-allowed transitions, which is discussed later in the paper.

system. Lattice parameters are plotted versus Ag and Ga fraction for both ternary and quaternary materials in Figure 3. With increasing Ga content, the lattice parameters a and c for the tetragonal unit cell decrease linearly, consistent with Vegard's law. However, with increasing Ag content, the lattice parameter a increases linearly, whereas the parameter c varies in a concave bowing fashion for all materials. A similar behavior of lattice parameters was reported by Matsushita et al. in the ternary $Ag_{1-x}Cu_xGaS_2$ system in 1993.[38] We hypothesize that this consistently observed behavior reflects the fact that the Cu and Ag may occupy slightly different positions within their S_4 coordination polyhedra in the mixed system, and further that the position offset may be more pronounced along the c-axis than in perpendicular directions, leading to a nonlinear variation of lattice parameter c but a linear change of parameter a versus the Ag to Cu ratio.

Figure 4 shows representative SEM images of $Ag_xCu_{1-x}Ga_yIn_{1-y}S_2$ semiconductor powders. The EDX elemental analysis was consistent with the initial elemental ratios in the starting materials, confirming the chemical components of the samples and the successful formation of the solid solutions. EDX mapping data in Figure 4C,D confirm the uniform distribution of the elemental constituents in the solid solutions. In the microstructural images, the sample in Figure 4A shows nanostructured edges with well-defined steps, whereas these features are absent in the Figure 4B sample. It has been suggested by Jang et al. that such nanostructures may improve the absorbance of scattered incident photons and the migration of photogenerated electrons.[26] This is consistent with our observation in the photocatalytic water reduction experiments described below.

Figure 5A shows the representative diffuse reflectance spectra of $Ag_{0.75}Cu_{0.25}Ga_yIn_{1-y}S_2$ $(0 \le y \le 1.0)$ semiconductors with the remaining spectra provided in Figures S6−S10. Weak absorption tails were observed in the spectra of some samples, which are associated with transitions from localized states in the band gap.[39] The band-gap values were derived from UV−vis diffuse reflectance spectroscopy by extrapolating the linear part of the $(\alpha h\nu)^2$ versus $h\nu$ based on the relation

$$\alpha h\nu = A(h\nu - E_g)^{1/2} \quad (1)$$

for direct transitions, where A is a constant and α is the absorption coefficient (cm^{-1}).[34,40] They are visually represented in Figure 5B—clearly showing that band-gap tuning is achieved by varying the Ag to Cu and Ga to In ratios. The band-gap variation versus Ag fraction for samples where y is equal to 0.25 is consistent with prior results for the limited stoichiometric study on $Ag_xCu_{1-x}Ga_{0.25}In_{0.75}S_2$ (x = 0, 0.1, 0.2, 0.3).[33] The variation in the band-gap values is visible to the eye, as the colors of $Ag_xCu_{1-x}Ga_yIn_{1-y}S_2$ powders change from dark green to yellow, orange, red purple, and finally black (Figure S11).

Although the change in band gap with the Ga/In ratio is relatively linear, as shown in Figure 5B, an unexpected nonlinear variation of band-gap values versus the Ag/Cu ratio is observed. This effect is most obvious when the IIIB site is totally populated with Ga, as seen in Figure 6 where the band gap is observed to hit a minimum at an Ag/Cu = 0.7, generating a "V-shaped" plot. This variation is unexpected in that the structure of the compounds follows Vegard's rule, but the band gap does not. In all cases, the pure Ag-based ternaries have larger band gaps than the samples containing Cu. At a fixed Cu to Ag ratio in the quaternary solid solutions, the band gap shows either a monotonic increase or decrease with Ga to In ratio. The unusual properties of the Ag-only samples compared to those with a small amount of Cu present suggest that one of the band energies is dominated by Cu states.

In an attempt to understand the underlaying electronic structure giving rise to the "V" shape of the band-gap variation, UPS experiments were carried out to determine the position of the VBM for the $Ag_xCu_{1-x}GaS_2$ semiconductors (see Figure S12). As shown in Figure 7, the trend of VBM energies generally follows the "V" shape, suggesting a second-order

DOI: 10.1021/acs.jpcc.8b05389
J. Phys. Chem. C 2018, 122, 24512−24519

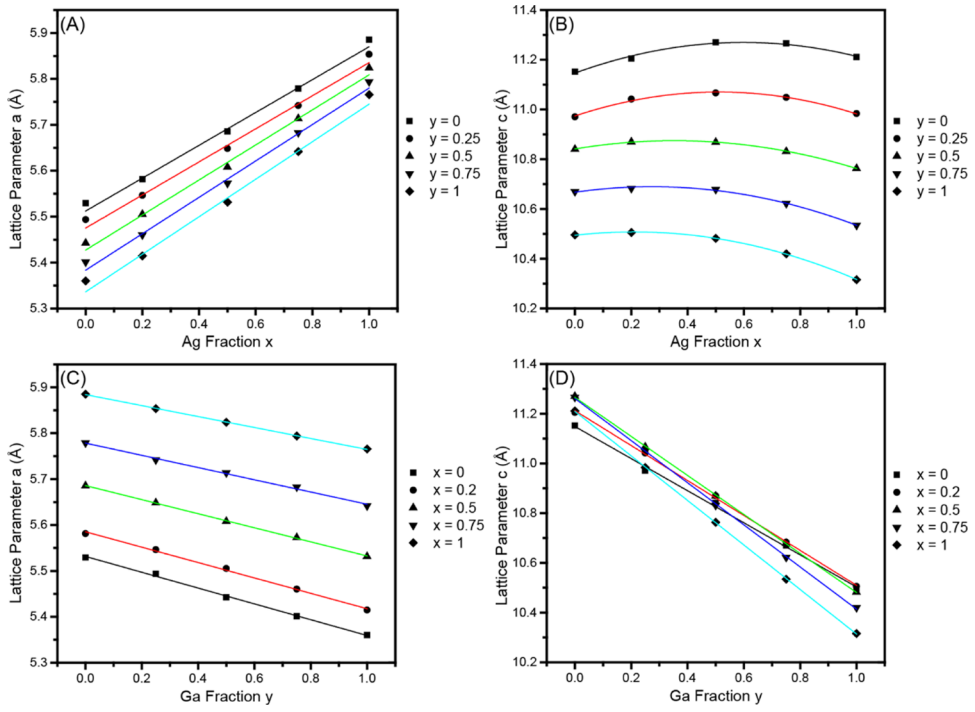

Figure 3. Correlation of tetragonal lattice parameters (a and c) with stoichiometry in the $Ag_xCu_{1-x}Ga_yIn_{1-y}S_2$ system. (A) Lattice parameter a versus mole fraction of silver, (B) lattice parameter c versus mole fraction of silver, (C) lattice parameter a vs mole fraction of gallium, and (D) lattice parameter c versus mole fraction of gallium.

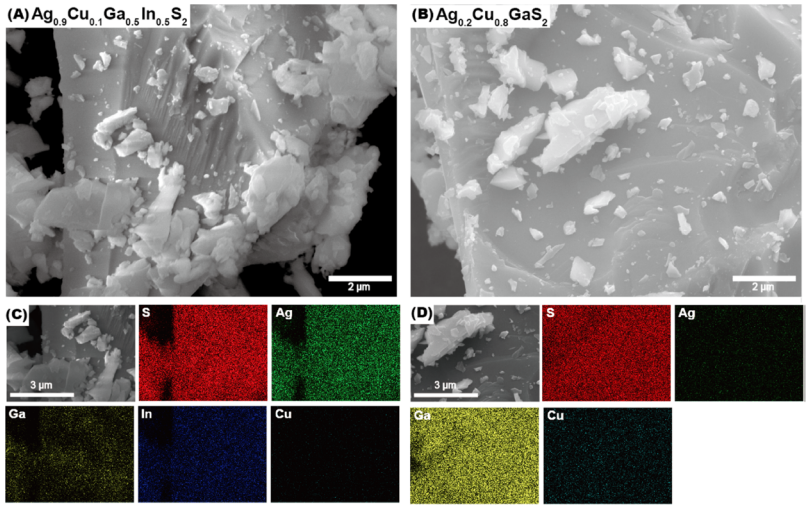

Figure 4. Representative SEM images of $Ag_xCu_{1-x}Ga_yIn_{1-y}S_2$: (A) $x = 0.9$, $y = 0.5$ and (B) $x = 0.2$, $y = 1$, with the corresponding EDX mapping in (C,D) respectively. (The dark area of the mapping in (C) corresponds to the left corner area in the original SEM image, where there is a void in the material.)

electronic phase change around $x = 0.7$. Overall, we find that the $Ag_xCu_{1-x}Ga_yIn_{1-y}S_2$ semiconductor materials have band gaps ranging from 1.3 to 2.5 eV, well-matched to the visible solar spectrum—supporting their potential applicability for photochemical water splitting.

Photochemical Water Reduction Using Ternary $Ag_xCu_{1-x}GaS_2$ ($0 \leq x \leq 1.0$) Powders with Sacrificial Electron Donors. Table 2 shows varying reaction conditions of $Ag_xCu_{1-x}GaS_2$ solid solutions for photocatalytic H_2 evolution using sulfur-containing electron donors under near-UV (365 nm) light. For non-Pt-loaded tests over $Ag_xCu_{1-x}GaS_2$ solid solutions (x = 1, 0.9, 0.8, 0.6, 0.4, 0.2, and 0), all Cu-doping candidates possessed little activity under the experimental conditions employed. $AgGaS_2$, however, with a H_2 evolution rate of 0.08 μmol h^{-1} g^{-1}, showed activity in the presence of Na_2SO_3 and Na_2S as sacrificial electron donors. Unfortunately, this material stopped producing H_2 after 4 h, suggesting photodegradation of the chalcopyrite. This conclusion was further supported by the observation of Ag_2S in a postphotolysis powder XRD pattern (Figure S13).

To optimize the activity of $Ag_xCu_{1-x}GaS_2$, a Pt-loading treatment (Table 2 entries 4, 6, and 7) was investigated for photocatalytic H_2 evolution. It has previously been noted in the $AgGaS_2$ system that a Pt co-catalyst serves as an active site for H_2 evolution, which not only facilitates H_2 production, but also increases the stability of $AgGaS_2$.[41] In the present

DOI: 10.1021/acs.jpcc.8b05389
J. Phys. Chem. C 2018, 122, 24512−24519

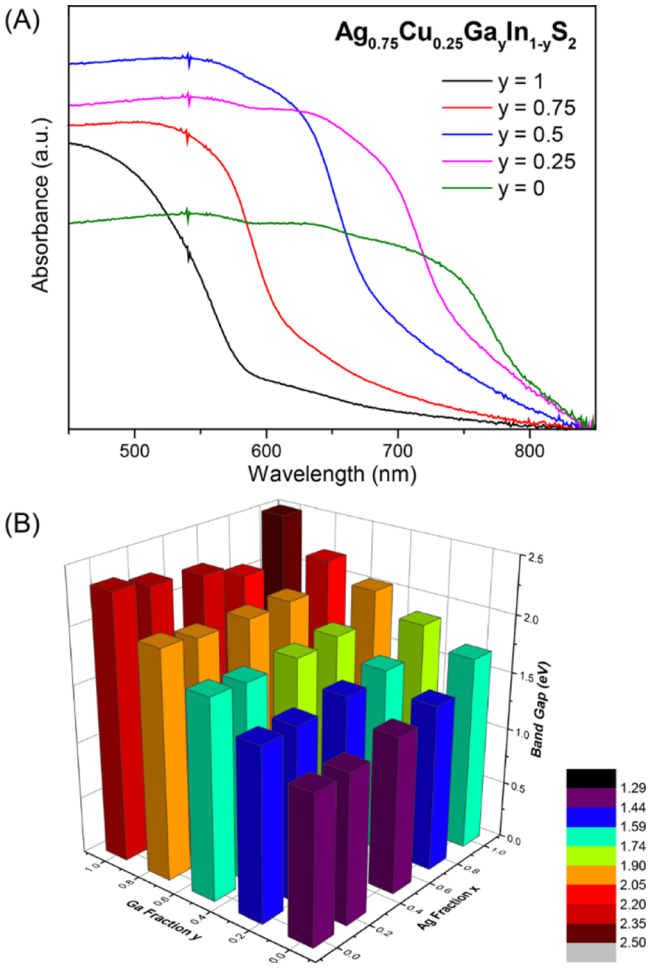

Figure 5. (A) Representative UV−vis absorbance spectra showing the effect of the Ga/In ratio in $Ag_{0.75}Cu_{0.25}Ga_yIn_{1-y}S_2$ on the optically observed band-gap energy. The absorbance data were Kubelka−Munk transformed from reflectance raw data; (B) optical band-gap values of $Ag_xCu_{1-x}Ga_yIn_{1-y}S_2$ semiconductors versus chemical composition (both Ag/Cu ratio and Ga/In ratio) as derived from optical spectra. Band-gap values are binned in 0.15 eV groups as shown by the colors.

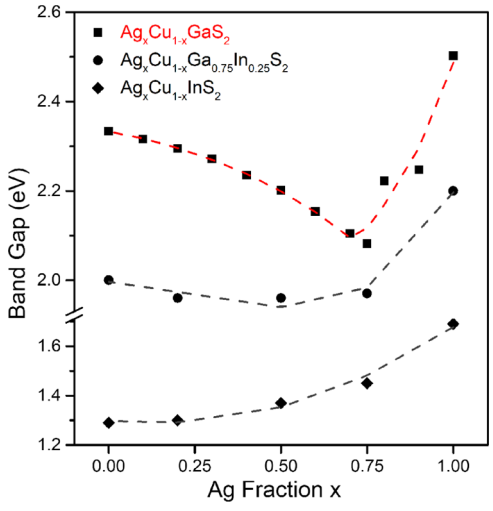

Figure 6. Band-gap values of $Ag_xCu_{1-x}Ga_yIn_{1-y}S_2$ semiconductors (y = 0, 0.75 and 1) vs Ag/Cu ratio as derived from the optical spectra. A unique "V" shape was revealed on the band-gap variation of $Ag_xCu_{1-x}GaS_2$.

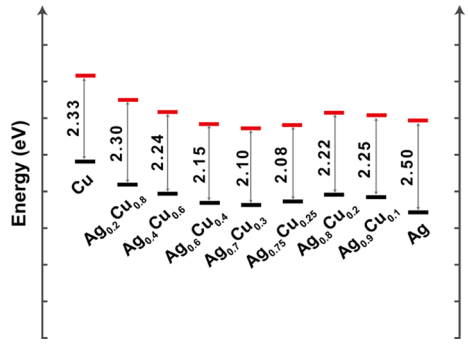

Figure 7. Relative valence band-edge energies (black, see Figure S12) of $Ag_xCu_{1-x}GaS_2$ semiconductors vs Ag fraction from UPS spectra along with band-gap values from diffuse reflectance measurements and calculated conduction band-edge energies (red).

experiments, Pt deposition was confirmed by XPS and SEM analysis of the postirradiated Pt-loaded $AgGaS_2$ (Figure S14). Addition of a platinum co-catalyst substantially increased the photocatalytic activity of $AgGaS_2$; further, the low activity Cu(I)-alloyed candidates were activated when platinum was introduced into the system. Interestingly, these activated candidates all lie on the right-hand branch of Figure 6, with high Ag content, whereas the left-branch samples, which are richer in copper, did not produce hydrogen even in the case of Pt deposition. Thus, the nonlinear variation of photocatalytic properties correlates with the unique "V" shape of the Ag-content-dependent band gap. In other words, doping Cu into $AgGaS_2$ in the left branch of the "V" shape (Figure 6) both increases the bandgap and hinders the photocatalytic activity of the semiconductor surface toward hydrogen evolution. A simple explanation for this effect could be a shift in the conduction band edge below the hydrogen redox potential as the system becomes copper-rich. However, this can be ruled out by the data in Figure 7 where it can be seen that the silver-rich branch of the data produces conduction band-edge energies that are lower than the conduction band-edge energies of the very copper-rich samples (far left of the diagram). For example, consider the x = 0.8 sample, which produces hydrogen and the x = 0.4 sample, which does not produce hydrogen even though both materials have conduction band energies that are the same within experimental error. Therefore, it appears that improved hydrogen evolution is not associated with the bulk electronic structure of the material, but rather is associated with improved interfacial charge transfer catalysis associated with the Ag-rich samples. This intriguing phenomenon is still under study, and its origin may lay the foundation of the relationship between the photocatalytic behavior and the band structures of these materials.

From a practical point of view, the use of platinum as a co-catalyst is not ideal. In addition to questions of sustainability, the activity of a platinum photocatalyst might change depending on the exact composition of the electrolyte employed. Thus, we explored the addition of sacrificial donors (sulfite and sulfide) that could enhance hydrogen evolution in the absence of a platinum catalyst.[5] The effects on the photocatalytic activity of $AgGaS_2$ obtained by varying the sulfur-containing reagent are presented in entries 2, 3, 5, 8, and 9 of Table 2. These results support the use of Na_2S as an electron donor, with a H_2 production rate of 0.94 μmol h^{-1} g^{-1}, in the absence of a Pt catalyst, and a H_2 production rate of

DOI: 10.1021/acs.jpcc.8b05389
J. Phys. Chem. C 2018, 122, 24512−24519

Table 2. Effects of Reaction and Preparation Condition on Photocatalytic H_2 Evolution Activities of $Ag_xCu_{1-x}GaS_2$ (x = 1, 0.9, and 0.8)

entry	sample name	reaction condition[d]	Pt-co-catalyst loading/wt %[c]	H_2 evolution rate (μmol h^{-1} g^{-1})
1	$AgGaS_2$	Na_2SO_3/Na_2S[a]	none	0.08
2	$AgGaS_2$	Na_2SO_3[b]	none	0.25
3	$AgGaS_2$	Na_2S[b]	none	0.94
4	$AgGaS_2$	Na_2SO_3/Na_2S[a]	0.5	1.25
5	$AgGaS_2$	Na_2S[b]	0.5	4.77
6	$Ag_{0.9}Cu_{0.1}GaS_2$	Na_2SO_3/Na_2S[a]	0.5	0.59
7	$Ag_{0.8}Cu_{0.2}GaS_2$	Na_2SO_3/Na_2S[a]	0.5	1.17
8	$Ag_{0.9}Cu_{0.1}GaS_2$	Na_2S[b]	0.5	4.65
9	$Ag_{0.8}Cu_{0.2}GaS_2$	Na_2S[b]	0.5	2.27

[a]A 15 mL vial containing ca. 22 mg of catalyst and 5 mL of 0.25 M Na_2SO_3/0.35 M Na_2S solution; light source: 3 W 365 nm LED light; irradiation area, 2.3 cm^2. [b]0.6 M electron donor was used. [c]The catalyst was treated with 0.5 wt % Pt loading by photodeposition of H_2PtCl_6 for 30 min, according to the literature method.[36,37] [d]The pH of all electrolytes employed was held constant at pH = 13.0 for all electrolyte combinations.

4.77 μmol h^{-1} g^{-1}, in the presence of platinum. The use of Na_2S as an optimized sacrificial electron donor was also supported by Meier et al. in 1984 with sulfides used for a water reduction system.[43,44]

Photocatalytical Water Reduction with Quaternary $Ag_xCu_{1-x}Ga_yIn_{1-y}S_2$ ($0 \le x \le 1.0$, $0 \le y \le 1.0$) Powders. Although improved performance of photocatalysis was observed by introducing a platinum co-catalyst, there is the concern that excess loading of the co-catalysts could decrease the system photocatalytic activity because of active site blocking and unwanted charge recombination.[5] In addition to the aforementioned band gap narrowing by adding Cu into $AgInS_2$, co-addition of Ga and Cu has also been predicted to improve the efficiency of $AgInS_2$ by continuously shifting the band-edge positions of both the VBM and CBM.[31,32] On the basis of these theoretical suggestions, the photocatalytic activities for H_2 evolution from (Ag,Cu)(Ga,In)S_2 are presented in Table 3. The ratio of Ga/In plays an essential role in improving the photocatalytic activity of Cu-doped $AgGaS_2$, which did not produce H_2 without the Pt co-catalyst in our tests. In particular, we note that $Ag_{0.75}Cu_{0.25}Ga_{0.25}In_{0.75}S_2$ demonstrates a catalytic performance comparable with that of Pt-loaded $Ag_xCu_{1-x}GaS_2$ (x = 1.0, 0.9 and 0.8) under the same experimental conditions (Table 2 entries 5, 8, and 9). A possible explanation for the improved activity is that the nanostructure features observed in Figure 4A may help incident photon absorption.[26,42]

Table 3. Photocatalytic Activities of $Ag_xCu_{1-x}Ga_yIn_{1-y}S_2$ (x = 0.9 and 0.75; y = 1, 0.8, 0.75, 0.5, 0.25, and 0.2)[a]

entry	sample name	H_2 evolution rate (μmol h^{-1} g^{-1})
1	$Ag_{0.9}Cu_{0.1}GaS_2$	0
2	$Ag_{0.9}Cu_{0.1}Ga_{0.8}In_{0.2}S_2$	1.43
3	$Ag_{0.9}Cu_{0.1}Ga_{0.5}In_{0.5}S_2$	1.49
4	$Ag_{0.9}Cu_{0.1}Ga_{0.2}In_{0.8}S_2$	1.20
5	$Ag_{0.75}Cu_{0.25}Ga_{0.75}In_{0.25}S_2$	2.90
6	$Ag_{0.75}Cu_{0.25}Ga_{0.5}In_{0.5}S_2$	2.24
7	$Ag_{0.75}Cu_{0.25}Ga_{0.25}In_{0.75}S_2$	3.15

[a]0.6 M Na_2S solution was used, and other conditions are the same as Table 2.

Besides the obviously increased hydrogen evolution rate, $Ag_{0.9}Cu_{0.1}Ga_yIn_{1-y}S_2$ samples with relatively high hydrogen evolution rates were confirmed to produce H_2 for at least 72 h without loss of activity. This suggests that greatly improved stability can be realized together with high efficiency for these quaternary semiconductors. The remarkable improvement of stability after adding a fourth cation into the system may be attributed to an inhibition in the quaternary system to the photodegradation of the semiconductors, mentioned in the previous section, and supported by postphotolysis XRD analysis of the samples showing no apparent degradation. Regarding practical application, the use of earth-abundant metals is more advantageous compared with noble-metal Pt. Therefore, the quaternary SCIGS semiconductors described here, with comparable water reduction efficiency and stability to the noble-metal-loaded ternaries as shown in Figure 8, will be of value for further exploration as photoelectrode materials in photoelectrochemistry (PEC) systems.

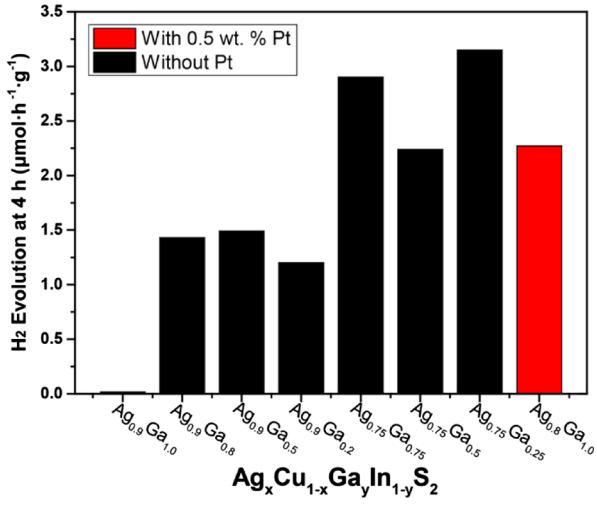

Figure 8. Hydrogen evolution rate at 4 h of quaternary $Ag_xCu_{1-x}Ga_yIn_{1-y}S_2$ (x = 0.9 and 0.75; y = 0.8, 0.75, 0.5, 0.25 and 0.2) together with ternary $Ag_{0.9}Cu_{0.1}GaS_2$ and $Ag_{0.8}Cu_{0.2}GaS_2$ for comparison; 0.6 M Na_2S solution was used; other conditions are the same as Table 2.

CONCLUSIONS

Quaternary $Ag_xCu_{1-x}Ga_yIn_{1-y}S_2$ ($0 \le x \le 1.0$ and $0 \le y \le 1.0$) semiconductor bulk materials have been prepared by the solid-state reaction method and their properties relevant to their use as water-spitting electrodes are reported for the first time. XRD spectra confirmed the formation of the chalcopyrite structure and SEM was employed to characterize the surface

DOI: 10.1021/acs.jpcc.8b05389
J. Phys. Chem. C 2018, 122, 24512−24519

morphologies of the materials. Both the VBM and CBM were variable in the solid solution, and the values of band gap, measured by diffuse reflectance spectroscopy, were found to range from 1.3 to 2.5 eV. A unique "V" shape was revealed in the band-gap variation of $Ag_xCu_{1-x}GaS_2$ and the quaternary systems versus Ag fraction, which is empirically related to their unexpected nonlinear behaviors in hydrogen evolution. Photocatalytic water reduction experiments were carried out on the materials in powder form with sacrificial electron donors, revealing that the quaternary semiconductor with composition near $Ag_{0.75}Cu_{0.25}Ga_{0.25}In_{0.75}S_2$ is able to reach, without noble-metal-loading, comparable performance to noble-metal-loaded ternary chalcopyrites. This quaternary material displays relatively high efficiency and high stability compared with the frequently studied ternary end members (i.e., $x = 0$ or $y = 0$) of the $Ag_xCu_{1-x}Ga_yIn_{1-y}S_2$ system, indicative of the potential of the quaternary system for PEC applications. Further study of the band structures and photocatalytic behavior of the SCIGS family, with the goal of understanding the relationship between these two properties is underway in our laboratories. However, at this point the correlation of bulk electronic structure with photocatalytic activity provides a new aspect of the semiconductor–electrolyte interface, which can be used to design improved water-splitting photoactive interfaces.

■ ASSOCIATED CONTENT

Supporting Information

The Supporting Information is available free of charge on the ACS Publications website at DOI: 10.1021/acs.jpcc.8b05389.

XRD patterns and UV–vis absorbance spectra of prepared semiconductors that are not included in the main text, a photograph showing the color change of the samples, the UPS spectra, the XRD pattern comparison of a sample pre- and postphotolysis, and the XPS and SEM analysis of the Pt-loaded sample (PDF)

■ AUTHOR INFORMATION

Corresponding Authors

*E-mail: rcava@princeton.edu (R.J.C.).

*E-mail: bocarsly@princeton.edu (A.B.B.).

ORCID

Hsin-Ya Kuo: 0000-0003-0194-3716

James Eujin Park: 0000-0003-2128-9811

Tia S. Lee: 0000-0003-0635-6668

Andrew B. Bocarsly: 0000-0003-3718-0933

Author Contributions

The paper was written through contributions of all the authors. All the authors have given approval to the final version of the paper.

Notes

The authors declare no competing financial interest.

■ ACKNOWLEDGMENTS

The authors acknowledge support of this research funding from the Office of Basic Energy Sciences, Department of Energy. The solid-state synthesis and material characterization were performed under the direction of R.J.C. (grant DE-FG02-98ER45706). Photochemical experiments were performed under the direction of A.B.B. (grant DE-SC0002133). We thank John Schreiber and Dr. Nan Yao for assistance with scanning electron microscopy, Yao-Wen Yeh for assistance with UPS measurements, and Prof. Gregory D. Scholes for assistance with diffuse reflectance spectroscopy.

■ REFERENCES

(1) Fujishima, A.; Honda, K. Electrochemical Photolysis of Water at a Semiconductor Electrode. *Nature* **1972**, *238*, 37–38.

(2) Kudo, A.; Miseki, Y. Heterogeneous photocatalyst materials for water splitting. *Chem. Soc. Rev.* **2009**, *38*, 253–278.

(3) Xing, C.; Zhang, Y.; Yan, W.; Guo, L. Band structure-controlled solid solution of Cd_{1-x} Zn_xS photocatalyst for hydrogen production by water splitting. *Int. J. Hydrogen Energy* **2006**, *31*, 2018–2024.

(4) Maeda, K.; Domen, K. Photocatalytic Water Splitting: Recent Progress and Future Challenges. *J. Phys. Chem. Lett.* **2010**, *1*, 2655–2661.

(5) Ran, J.; Zhang, J.; Yu, J.; Jaroniec, M.; Qiao, S. Z. Earth-abundant cocatalysts for semiconductor-based photocatalytic water splitting. *Chem. Soc. Rev.* **2014**, *43*, 7787–7812.

(6) Yerga, R. M. N.; Galván, M. C. Á.; del Valle, F.; de la Mano, J. A.; Fierro, J. L. G. Water Splitting on Semiconductor Catalysts under Visible-Light Irradiation. *ChemSusChem* **2009**, *2*, 471–485.

(7) Wolcott, A.; Smith, W. A.; Kuykendall, T. R.; Zhao, Y.; Zhang, J. Z. Photoelectrochemical Study of Nanostructured ZnO Thin Films for Hydrogen Generation from Water Splitting. *Adv. Funct. Mater.* **2009**, *19*, 1849–1856.

(8) Yang, X.; Wolcott, A.; Wang, G.; Sobo, A.; Fitzmorris, R. C.; Qian, F.; Zhang, J. Z.; Li, Y. Nitrogen-Doped ZnO Nanowire Arrays for Photoelectrochemical Water Splitting. *Nano Lett.* **2009**, *9*, 2331–2336.

(9) Lin, Y.-G.; Hsu, Y.-K.; Chen, Y.-C.; Chen, L.-C.; Chen, S.-Y.; Chen, K.-H. Visible-light-driven photocatalytic carbon-doped porous ZnO nanoarchitectures for solar water-splitting. *Nanoscale* **2012**, *4*, 6515–6519.

(10) Sayama, K.; Nomura, A.; Arai, T.; Sugita, T.; Abe, R.; Yanagida, M.; Oi, T.; Iwasaki, Y.; Abe, Y.; Sugihara, H. Photoelectrochemical Decomposition of Water into H_2 and O_2 on Porous $BiVO_4$ Thin-Film Electrodes under Visible Light and Significant Effect of Ag Ion Treatment. *J. Phys. Chem. B* **2006**, *110*, 11352–11360.

(11) Ye, H.; Lee, J.; Jang, J. S.; Bard, A. J. Rapid Screening of $BiVO_4$-Based Photocatalysts by Scanning Electrochemical Microscopy (SECM) and Studies of Their Photoelectrochemical Properties. *J. Phys. Chem. C* **2010**, *114*, 13322–13328.

(12) Iwase, A.; Kudo, A. Photoelectrochemical water splitting using visible-light-responsive $BiVO_4$ fine particles prepared in an aqueous acetic acid solution. *J. Mater. Chem.* **2010**, *20*, 7536–7542.

(13) Kim, T. W.; Choi, K.-S. Nanoporous $BiVO_4$ Photoanodes with Dual-Layer Oxygen Evolution Catalysts for Solar Water Splitting. *Science* **2014**, *343*, 990.

(14) Abdi, F. F.; Han, L.; Smets, A. H. M.; Zeman, M.; Dam, B.; van de Krol, R. Efficient solar water splitting by enhanced charge separation in a bismuth vanadate-silicon tandem photoelectrode. *Nat. Commun.* **2013**, *4*, 2195.

(15) Hwang, D. W.; Kim, J.; Park, T. J.; Lee, J. S. Mg-Doped WO_3 as a Novel Photocatalyst for Visible Light-Induced Water Splitting. *Catal. Lett.* **2002**, *80*, 53–57.

(16) Miller, E. L.; Marsen, B.; Cole, B.; Lum, M. Low-Temperature Reactively Sputtered Tungsten Oxide Films for Solar-Powered Water Splitting Applications. *Electrochem. Solid-State Lett.* **2006**, *9*, G248–G250.

(17) Hong, S. J.; Jun, H.; Borse, P. H.; Lee, J. S. Size effects of WO_3 nanocrystals for photooxidation of water in particulate suspension and photoelectrochemical film systems. *Int. J. Hydrogen Energy* **2009**, *34*, 3234–3242.

(18) Arriaga, L. G.; Fernández, A. M.; Solorza, O. Preparation and characterization of (Zn,Cd)S photoelectrodes for hydrogen production. *Int. J. Hydrogen Energy* **1998**, *23*, 995–998.

(19) Zhang, J.; Wang, L.; Liu, X.; Li, X.; Huang, W. High-performance CdS–ZnS core–shell nanorod array photoelectrode for

DOI: 10.1021/acs.jpcc.8b05389
J. Phys. Chem. C 2018, 122, 24512–24519

photoelectrochemical hydrogen generation. *J. Mater. Chem. A* **2015**, *3*, 535−541.
(20) Abe, R.; Higashi, M.; Domen, K. Facile Fabrication of an Efficient Oxynitride TaON Photoanode for Overall Water Splitting into H_2 and O_2 under Visible Light Irradiation. *J. Am. Chem. Soc.* **2010**, *132*, 11828−11829.
(21) Park, J. E.; Hu, Y.; Krizan, J. W.; Gibson, Q. D.; Tayvah, U. T.; Selloni, A.; Cava, R. J.; Bocarsly, A. B. Stable Hydrogen Evolution from an $AgRhO_2$ Photocathode under Visible Light. *Chem. Mater.* **2018**, *30*, 2574−2582.
(22) Gu, J.; Yan, Y.; Krizan, J. W.; Gibson, Q. D.; Detweiler, Z. M.; Cava, R. J.; Bocarsly, A. B. p-Type $CuRhO_2$ as a Self-Healing Photoelectrode for Water Reduction under Visible Light. *J. Am. Chem. Soc.* **2014**, *136*, 830−833.
(23) Maeda, K. Photocatalytic water splitting using semiconductor particles: History and recent developments. *J. Photochem. Photobiol., C* **2011**, *12*, 237−268.
(24) Kudo, A. Development of photocatalyst materials for water splitting. *Int. J. Hydrogen Energy* **2006**, *31*, 197−202.
(25) (a) Tsuji, I.; Kato, H.; Kobayashi, H.; Kudo, A. Photocatalytic H_2 Evolution under Visible-Light Irradiation over Band-Structure-Controlled $(CuIn)_xZn_{2(1-x)}S_2$ Solid Solutions. *J. Phys. Chem. B* **2005**, *109*, 7323−7329. (b) Frick, J. J.; Kushwaha, S. K.; Cava, R. J.; Bocarsly, A. B. Characterization of Primary Carrier Transport Properties of the Light-Harvesting Chalcopyrite Semiconductors $CuIn(S_{1-x}Se_x)_2$. *J. Phys. Chem. C* **2017**, *121*, 17046−17052. (c) Frick, J. J.; Cava, R. J.; Bocarsly, A. B. Chalcopyrite $CuIn(S_{1-x}Se_x)_2$ for Photoelectrocatalytic H_2 Evolution: Unraveling the Energetics and Complex Kinetics of Photogenerated Charge Transfer in the Semiconductor Bulk. *Chem. Mater.* **2018**, *30*, 4422−4431.
(26) Jang, J. S.; Borse, P. H.; Lee, J. S.; Choi, S. H.; Kim, H. G. Indium induced band gap tailoring in $AgGa_{1-x}In_xS_2$ chalcopyrite structure for visible light photocatalysis. *J. Chem. Phys.* **2008**, *128*, 154717.
(27) Kaga, H.; Tsutsui, Y.; Nagane, A.; Iwase, A.; Kudo, A. An effect of Ag(I)-substitution at Cu sites in $CuGaS_2$ on photocatalytic and photoelectrochemical properties for solar hydrogen evolution. *J. Mater. Chem. A* **2015**, *3*, 21815−21823.
(28) Luo, J.; Tilley, S. D.; Steier, L.; Schreier, M.; Mayer, M. T.; Fan, H. J.; Grätzel, M. Solution Transformation of Cu_2O into $CuInS_2$ for Solar Water Splitting. *Nano Lett.* **2015**, *15*, 1395−1402.
(29) Zhang, L.; Minegishi, T.; Nakabayashi, M.; Suzuki, Y.; Seki, K.; Shibata, N.; Kubota, J.; Domen, K. Durable hydrogen evolution from water driven by sunlight using $(Ag,Cu)GaSe_2$ photocathodes modified with CdS and $CuGa_3Se_5$. *Chem. Sci.* **2015**, *6*, 894−901.
(30) Stanbery, B. J. Copper Indium Selenides and Related Materials for Photovoltaic Devices. *Crit. Rev. Solid State Mater. Sci.* **2002**, *27*, 73−117.
(31) Huang, D.; Ju, Z.; Ning, H.; Li, C.; Yao, C.; Guo, J. First-principles study on $CuAlTe_2$ and $AgAlTe_2$ for water splitting. *Mater. Chem. Phys.* **2014**, *148*, 882−886.
(32) Huang, D.; Persson, C. Photocatalyst $AgInS_2$ for active overall water-splitting: A first-principles study. *Chem. Phys. Lett.* **2014**, *591*, 189−192.
(33) Septina, W.; Sugimoto, M.; Chao, D.; Shen, Q.; Nakatsuka, S.; Nose, Y.; Harada, T.; Ikeda, S. Photoelectrochemical Water Reduction over Wide Gap $(Ag,Cu)(In,Ga)S_2$ Thin Film Photocathodes. *Phys. Chem. Chem. Phys.* **2017**, *19*, 12502−12508.
(34) Tarasova, A. Y.; Isaenko, L. I.; Kesler, V. G.; Pashkov, V. M.; Yelisseyev, A. P.; Denysyuk, N. M.; Khyzhun, O. Y. Electronic structure and fundamental absorption edges of KPb_2Br_5, $K_{0.5}Rb_{0.5}Pb_2Br_5$, and $RbPb_2Br_5$ single crystals. *J. Phys. Chem. Solids* **2012**, *73*, 674−682.
(35) Tinker, L. L.; McDaniel, N. D.; Curtin, P. N.; Smith, C. K.; Ireland, M. J.; Bernhard, S. Visible Light Induced Catalytic Water Reduction without an Electron Relay. *Chem.—Eur. J.* **2007**, *13*, 8726−8732.
(36) Kraeutler, B.; Bard, A. J. Heterogeneous Photocatalytic Preparation of Supported Catalysts. Photodeposition of Platinum on Titanium Dioxide Powder and Other Substrates. *J. Am. Chem. Soc.* **1978**, *100*, 4317−4318.
(37) Lin, P.-C.; Wang, P.-Y.; Li, Y.-Y.; Hua, C. C.; Lee, T.-C. Enhanced photocatalytic hydrogen production over In-rich (Ag−In−Zn)S particles. *Int. J. Hydrogen Energy* **2013**, *38*, 8254−8262.
(38) Matsushita, H.; Endo, S.; Irie, T. Structural and Optical Properties of the $Cu_{1-x}Ag_xGaS_2$ System. *Jpn. J. Appl. Phys.* **1993**, *32*, L1049−L1050.
(39) Wood, D. L.; Tauc, J. Weak Absorption Tails in Amorphous Semiconductors. *Phys. Rev. B: Solid State* **1972**, *5*, 3144−3151.
(40) Chavhan, S.; Sharma, R. Growth, structural and optical properties of non-stoichiometric $CuIn(S_{1-x}Se_x)_2$ thin films deposited by solution growth technique for photovoltaic application. *J. Phys. Chem. Solids* **2006**, *67*, 767−773.
(41) Tsuji, I.; Kato, H.; Kobayashi, H.; Kudo, A. Photocatalytic H_2 Evolution Reaction from Aqueous Solutions over Band Structure-Controlled $(AgIn)_xZn_{2(1-x)}S_2$ Solid Solution Photocatalysts with Visible-Light Response and Their Surface Nanostructures. *J. Am. Chem. Soc.* **2004**, *126*, 13406−13413.
(42) Chen, S.; Gong, X. G.; Wei, S.-H. Band-structure anomalies of the chalcopyrite semiconductors $CuGaX_2$ versus $AgGaX_2$ (X = S and Se) and their alloys. *Phys. Rev. B: Condens. Matter Mater. Phys.* **2007**, *75*, 205209.
(43) Buehler, N.; Meier, K.; Reber, J. F. Photochemical hydrogen production with cadmium sulfide suspensions. *J. Phys. Chem.* **1984**, *88*, 3261−3268.
(44) Reber, J. F.; Meier, K. Photochemical production of hydrogen with zinc sulfide suspensions. *J. Phys. Chem.* **1984**, *88*, 5903−5913.

DOI: 10.1021/acs.jpcc.8b05389
J. Phys. Chem. C 2018, 122, 24512−24519